Applications and Applied Mathematics: An International Journal (AAM)

Volume 13 | Issue 2 Article 14

12-2018

The Circular Restricted Four-body Problem With Triaxial Primaries and Variable Infinitesimal Mass

Abdullah A. Ansari
Majmaah University

Available at
http://pvamu.edu/aam
Appl. Appl. Math.
ISSN: 1932-9466

Applications and Applied Mathematics:
An International Journal
(AAM)

Vol. 13, Issue 2 (December 2018), pp. 818 – 838

The Circular Restricted Four-body Problem With Triaxial Primaries and Variable Infinitesimal Mass

Abdullah A. Ansari

Department of Mathematics
College of Science Al-Zulfi
Majmaah University
Kingdom of Saudi Arabia
a.ansari@mu.edu.sa

Received: February 14, 2018; Accepted: November 7, 2018

Abstract

This paper investigates the circular restricted four-body problem in which three primaries are taken as triaxial rigid body which are placed at the vertices of an equilateral triangle and the fourth infinitesimal body is varying its mass with time. We used the Jeans law to determine equations of motion and then evaluated the Jacobi integral. In the next section, we have performed the computational work to draw the graphs of the equilibrium points in different planes, zero velocity curves, surfaces and the Newton-Raphson basins of attraction with the variations of the triaxiality parameters. Finally, we have examined the linear stability of the equilibrium points with the help of Meshcherskii space-time inverse transformation and found that all the equilibrium points are unstable.

Keywords: Circular Restricted Problem; Equilateral Triangle; Triaxial Body; Variable Mass; Zero-velocity Curves; Surfaces; Basins of Attraction

MSC 2010 No.: 70F15, 85A20, 70F05

1. Introduction

The restricted four-body problem is an interesting and attracting problem for scientists in the space dynamics since many decades. In these four bodies, one body is taken very small known as infinitesimal body and the rest three bodies are primaries. The infinitesimal body is moving in the gravitational forces of these three primaries but it is not influencing them. There are two types

of configurations. Firstly, the Eularian configuration in which the three primaries are placed in a straight line. Secondly, the Lagrangian configuration in which the three primaries are placed at the vertices of an equilateral triangle. This configuration is also known as equilateral triangular configuration or central configuration since the accelerations of the primaries are proportional to the corresponding radius vectors. A simplest example of the restricted four-body problem can be seen in the Sun-Earth-Moon-Spacecraft System.

Many scientists have studied the restricted problem with different perturbations as shapes of the bodies (oblate as well as triaxial), resonance, variable mass of the primaries as well as infinitesimal body, Coriolis and centrifugal forces, Pointing-Robertson drag, solar radiation pressure and albedo effects etc. Simo (1978) investigated the linear stability of the relative lagrangian solutions in the four-body problem. Hadjidemetriou (1980) studied the periodic orbits of fourth body in the restricted four-body problem with respect to rotating frame. Kalvouridis et al. (1995, 1997, 2006) investigated the equilibrium points and stability in the restricted four-body problem under the effect of oblateness and radiation pressure. And also performed the zero-velocity surface and curves. Baltagiannis et al. (2011) shown that equilibrium points depend on the mass of the primaries in the restricted four-body problem. Papadauris et al. (2013, 2014) investigated the existence, locations, stability and periodic orbits of the equilibrium points in and out of the orbital plane in the photogravitational circular restricted four-body problem. Kumari et al. (2013) analyzed the motion of an infinitesimal mass in the restricted four-body problem with solar wind drag and drawn the zero-velocity surfaces. And also they have examined the stability with the help of Poincaré surface of section and Lyapunov characteristic exponent.

Abdullah (2014) studied the periodic orbits in the restricted four-body problem around lagrangian points in three cases. In the first case, he has considered all three primaries as spherical in shape. In the second case, he has taken one of the three primaries as an oblate body. And in the third and last case, he has taken two of the primaries as oblate body and all the three primaries are source of radiation pressure. Papadakis (2016) performed the 21 families of simple 3D symmetric periodic orbits as well as the typical orbits of all symmetry type 3D orbits in the circular restricted four-body problem. After examined the stability, he illustrated the characteristic curves and stability diagrams of families of 3D periodic orbits. Asique et al. (2015 (a, b), 2016, 2017) studied the restricted four-body problem with different shapes of the primaries with solar radiation pressure. They have placed one of the primaries at the lagrangian points of the classical restricted three-body problem. They have illustrated the equilibrium points and zero-velocity curves for these models. Singh et al. (2016 (a, b)) investigated in and out of plane equilibrium points in the circular restricted four-body problem with the effect of solar radiation pressure. Suraj et al. (2017) have studied the planar equilateral restricted four-body problem with the effect of triaxial parameters. And illustrated the libration points, zero-velocity curves, zero-velocity surfaces with projections and Newton-Raphson basins of attraction of the problem.

Many scientists have investigated on these models with variable masses, such as Jeans (1928), Meshcherskii (1952), Shrivastava (1983), Lichtenegger (1984), Singh (1984, 1985, 2003, 2010, 2013), Lukyanov (2009), Zhang (2012), Abouelmagd (2015), Mittal (2016), Ansari (2016 (a, b, c), 2017 (a, b), 2018), etc. Also, many scientists have explained the basins of attraction in these models as Douskos (2010), Kumari (2014), Ansari (2016 (c), 2017 (a, b), Zotos (2016 (a, b, c),

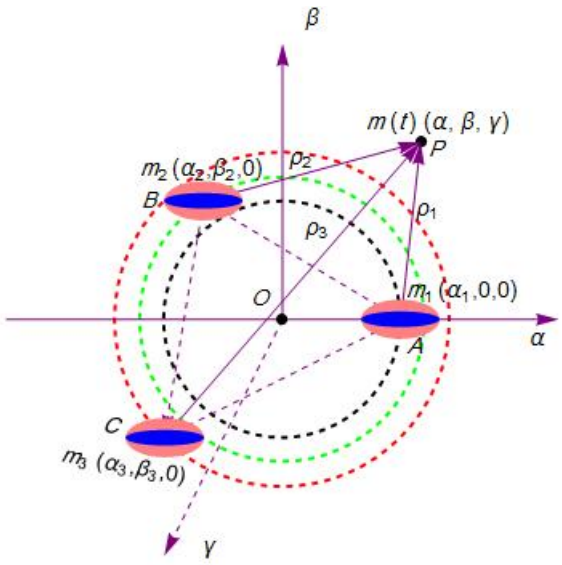

Figure 1. Geometric configuration of the problem.

2017, 2018), etc.

After reviewing the literature, we have decided to study the motion of the infinitesimal variable body in the frame of the circular restricted four-body problem in which three primaries are taken as equal triaxial. We have explored the problem in various sections. In the statement of the problem and equations of motion section, we have derived the equations of motion of the infinitesimal variable mass under the triaxial primaries having equal masses and also determined the Jacobi-Integral. In the numerical analysis section, we have plotted the equilibrium points in different three planes, the zero-velocity curves, surfaces and the Newton-Raphson basins of attraction through Mathematica software. In the stability section, we have examined the stability of the equilibrium points under the effect of triaxiality parameters and variation of mass parameter. Finally, we have concluded the problem.

2. Statement of the problem and equations of motion

Let there be three triaxial primaries of equal masses $(m_1 = m_2 = m_3)$, placed at the vertices of an equilateral triangle ABC and moving in the circular orbits around their common center of mass which is taken as origin O, in the same plane. Let the coordinates of A, B, C and P be $(\xi_i, \eta_i, 0), (i = 1, 2, 3)$ and (ξ, η, ζ) respectively in synodic coordinate system and $AB = l$. The fourth variable mass $m(t)$ is moving in the space under the influence of these three primaries but not influencing them (Figure 1).

Following the procedure given by Mittal (2016) and Suraj (2017) and taking the unit of mass, length and time such that $m_1 + m_2 + m_3 = 1, l = 1$ and $G = 1$, respectively and also the angular velocity $\omega = 1$ (Pandey 2016), we can write the equations of motion of the infinitesimal variable mass in the synodic coordinate system when the variation of mass is non-isotropic and originates from one

point as

$$\begin{cases} \frac{\dot{m}(t)}{m(t)}(\dot{\xi}-\eta)+(\ddot{\xi}-2\dot{\eta})=\Omega_{\xi}, \\ \frac{\dot{m}(t)}{m(t)}(\dot{\eta}+\xi)+(\ddot{\eta}+2\dot{\xi})=\Omega_{\eta}, \\ \frac{\dot{m}(t)}{m(t)}\dot{\zeta}+\ddot{\zeta}=\Omega_{\zeta}, \end{cases} \tag{1}$$

where

$$\begin{cases} \Omega=\frac{1}{2}(\xi^2+\eta^2)+\sum_{i=1}^{3}[\frac{1}{3r_i}+\frac{(\lambda_1+\lambda_2)}{6r_i^3}-\frac{(\lambda_1(\eta-\eta_i)^2+\lambda_2\zeta^2)}{2r_i^5}], \\ r_i^2=(\xi-\xi_i)^2+(\eta-\eta_i)^2+\zeta^2, \\ \lambda_1=\frac{(a^2-b^2)}{5l^2}, \lambda_2=\frac{(a^2-c^2)}{5l^2}. \end{cases} \tag{2}$$

Here dot represents differentiation with respect to time. Also λ_1, λ_2 are triaxiality parameters and a, b, c are semi-axes of triaxial rigid bodies.

We will use Jean's law for the variable infinitesimal body as

$$\frac{dm}{dt}=-\lambda_3 m^n, \tag{3}$$

where λ_3 is constant and the value of exponent n is within the limit $0.4 \leqslant n \leqslant 4.4$ (for the stars). For a rocket, n = 1, and the mass of the rocket varies exponentially as $m=m_0e^{-\lambda_3 t}, m_0$ is the initial mass.

By using the space time transformations

$$\alpha=\epsilon^q\xi, \beta=\epsilon^q\eta, \gamma=\epsilon^q\zeta, d\Gamma=\epsilon^k dt, \rho_i=\epsilon^q r_i, (i=1,2,3),$$

where $\epsilon=\frac{m}{m_0}$.

The equations of motion (1), under the assumptions $q=\frac{1}{2}, k=0, n=1$ become

$$\begin{cases} \ddot{\alpha}-2\dot{\beta}=\psi_{\alpha}, \\ \ddot{\beta}+2\dot{\alpha}=\psi_{\beta}, \\ \ddot{\gamma}=\psi_{\gamma}, \end{cases} \tag{4}$$

where

$$\begin{cases} \psi & = \frac{1}{2}(\alpha^2+\beta^2)+\frac{\lambda_3^2}{8}(\alpha^2+\beta^2+\gamma^2) \\ & \quad +\sum_{i=1}^{3}[\frac{\epsilon^{3/2}}{3\rho_i}+\frac{\epsilon^{5/2}(\lambda_1+\lambda_2)}{6\rho_i^3}-\frac{\epsilon^{5/2}(\lambda_1(\beta-\beta_i)^2+\lambda_2\gamma^2)}{2\rho_i^5}], \\ \rho_i^2 & = (\alpha-\alpha_i)^2+(\beta-\beta_i)^2+\gamma^2, \\ (\alpha_1,\beta_1) & = (\frac{\lambda}{\sqrt{3}},0),(\alpha_2,\beta_2)=(\frac{-\lambda}{2\sqrt{3}},\frac{\lambda}{2}), \\ (\alpha_3,\beta_3) & = (\frac{-\lambda}{2\sqrt{3}},\frac{-\lambda}{2}),\lambda=1+\frac{1}{4}(\lambda_1+\lambda_2). \end{cases} \tag{5}$$

From Equation (4), we can evaluate the Jacobian integral as

$$\dot{\alpha}^2+\dot{\beta}^2+\dot{\gamma}^2=2\psi-C, \tag{6}$$

where C is the Jacobi Integral constant which is conserved and related to the total energy of the system. The curve for a given values of the energy integral is restricted in its motion to regions in which $C \geqslant 2\psi(\alpha,\beta)$, and all other regions are prohibited to the fourth infinitesimal body i.e., the velocities will be zero in these regions.

3. Numerical Analysis

We have examined the effect of triaxiality on equilibrium points, zero-velocity curves, surfaces and basins of attraction by plotting their graphs numerically. (in all the calculations $\lambda_3 = 0.2, \epsilon = 0.1$.)

3.1. Equilibrium points

The solutions of right hand side of Equation (4) will be the location of equilibrium points. We have examined the effect of triaxiality on collinear equilibrium points$(\alpha \neq 0, \beta = 0, \gamma = 0)$ (Figure 2, Figure 3), non-collinear equilibrium points $(\alpha \neq 0, \beta \neq 0, \gamma = 0)$ (Figure 4, Figure 5) and out-of plane equilibrium points ($(\alpha \neq 0, \beta = 0, \gamma \neq 0)$ and $(\alpha = 0, \beta \neq 0, \gamma \neq 0)$) (Figure 6, Figure 7, Figure 8, Figure 9). At the equilibrium points, all the derivatives of the co-ordinates with respect to the time will be zero i.e., velocities and accelerations will be zero. We have

$$\begin{cases} \psi_\alpha = 0, & (a) \\ \psi_\beta = 0, & (b) \\ \psi_\gamma = 0. & (c) \end{cases} \tag{7}$$

3.1.1. *Collinear equilibrium points*

The collinear equilibrium points are the solutions of the Equations (7a) when $\beta = 0$ and $\gamma = 0$ and it will lie on the $\alpha-$axis. We obtained only two collinear equilibrium points when all the three

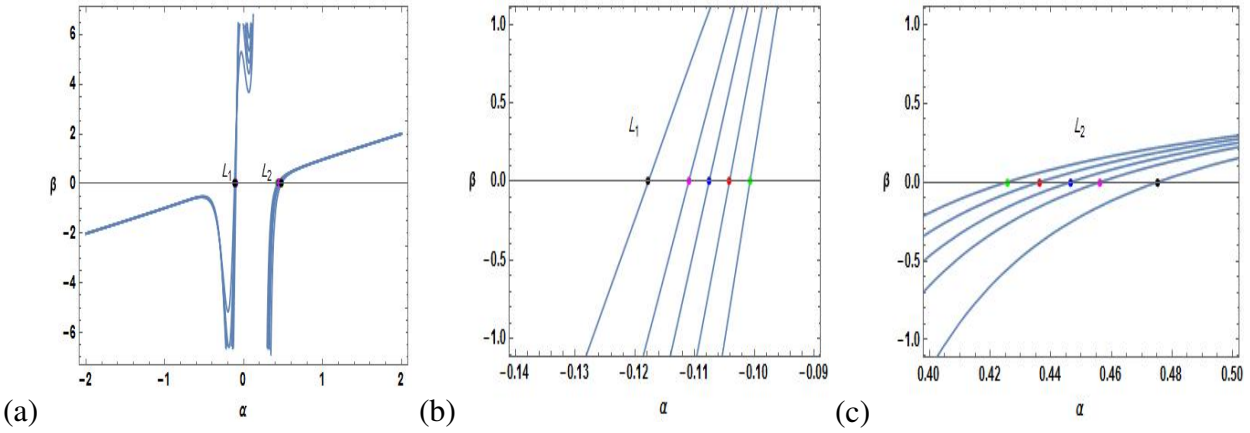

Figure 2. (a): Locations of collinear equilibrium points at the values of triaxiality parameter $\lambda_1(= 0.05(Green), 0.1(Red), 0.15(Blue), 0.2(Magenta), 0.3(Black))$ and $\lambda_2 = 0.25$, (b, c): The zoomed part of figure (a) near L_1 and L_2 respectively.

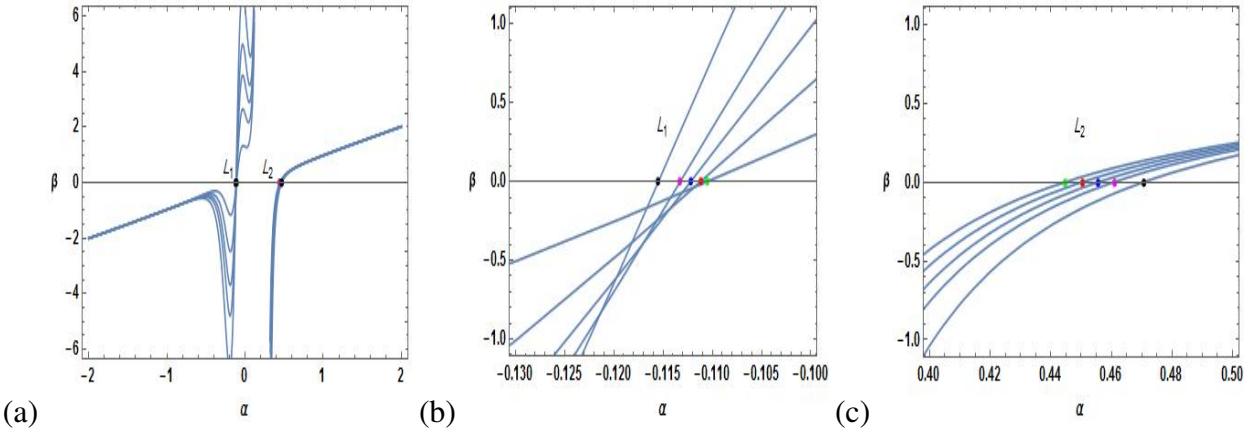

Figure 3. (a): Locations of collinear equilibrium points at the values of triaxiality parameter $\lambda_1 = 0.25$ and $\lambda_2(= 0.05(Green), 0.1(Red), 0.15(Blue), 0.2(Magenta), 0.3(Black))$, (b, c): The zoomed part of figure (a) near L_1 and L_2 respectively.

primaries are triaxial rigid bodies with equal masses and mass of the infinitesimal body varies with time. From the Figures (2a, 3a), there are two collinear equilibrium points L_1 and L_2. We also observed that as we increase the values of triaxiality parameter $\lambda_1(= 0.05, 0.1, 0.15, 0.2, 0.3)$ by keeping $\lambda_2 = 0.25$, both the equilibrium points L_1 (Figure 2b) and L_2 (Figure 2c) move away from the origin. And also we observed the same phenomenon when we increase the values of triaxiality parameter $\lambda_2(= 0.05, 0.1, 0.15, 0.2, 0.3)$ by keeping $\lambda_1 = 0.25$ (Figure 3). We have given some values of equilibrium points in the Tables 1 and 2.

3.1.2. *Non-Collinear equilibrium points*

Non-collinear equilibrium points are the solutions of Equations $(7a)$ and $(7b)$. In the case when all the primaries have equal mass i.e. $m_1 = m_2 = m_3 = \frac{1}{3}$, and are triaxial in shape and also

Table 1. Coordinates of Collinear and Non-collinear equilibrium points when the primaries are triaxial rigid body with equal mass ($\lambda_2 = 0.25$).

λ_1	L_1	L_2	L_3	L_4
0.05	(-0.110557, 0)	(0.444717, 0)	–	–
0.10	(-0.111210, 0)	(0.450360, 0)	–	–
0.15	(-0.112202, 0)	(0.455742, 0)	(0.220206, 0.089374)	(0.220206, -0.089374)
0.20	(-0.113270, 0)	(0.460906, 0)	(0.190086, 0.130063)	(0.190086, -0.130063)
0.30	(-0.115477, 0)	(0.470703, 0)	(0.169659, 0.127267)	(0.169659, -0.127267)

Table 2. Coordinates of Collinear and Non-collinear equilibrium points when the primaries are triaxial rigid body with equal mass ($\lambda_1 = 0.25$).

λ_2	L_1	L_2	L_3	L_4
0.05	(-0.100716, 0)	(0.425624, 0)	(0.133097, 0.102523)	(0.133097, -0.102523)
0.10	(-0.104147, 0)	(0.436244, 0)	(0.142178, 0.109269)	(0.142178, -0.109269)
0.15	(-0.107567, 0)	(0.446443, 0)	(0.152138, 0.116128)	(0.152138, -0.116128)
0.20	(-0.113270, 0)	(0.456303, 0)	(0.163245, 0.122934)	(0.163245, -0.122934)
0.30	(-0.117740, 0)	(0.475232, 0)	(0.190899, 0.134455)	(0.190899, -0.134455)

the mass of the infinitesimal body varies with time, we got at most four equilibrium points. As increase the value of the triaxial parameter $\lambda_1(= 0.05, 0.1, 0.15, 0.2, 0.3)$ and $\lambda_2 = 0.25$, there exist at most four equilibrium points (L_1, L_2, L_3, L_4). At $\lambda_1 = 0.05, 0.1$, there exist only two equilibrium points (L_1, L_2) (Figure 4a, 4b) but at $\lambda_1 = 0.15, 0.2, 0.3$, there exist four equilibrium points (L_1, L_2, L_3, L_4) (Figure 4c). The Figure 4d is the zoomed part of the Figure 4c near L_3. We found that as increase the value of $\lambda_1(= 0.15, 0.2, 0.3)$ the equilibrium points $L_{1,2}$ move away from primary m_1 while the equilibrium points $L_{3,4}$ move toward the primary m_1. And also as increase the value of the $\lambda_2(= 0.05, 0.1, 0.15, 0.2, 0.3)$ and $\lambda_1 = 0.25$, there exist at most four equilibrium points (L_1, L_2, L_3, L_4)(Figure 5a). The Figure 5b is the zoomed part of the Figure 5a near L_3. We found that as increase the value of λ_2 the equilibrium points $L_{1,2}$ move away from m_1 while the equilibrium points $L_{3,4}$ move toward the primary m_1. In all the figures of this section, purple color points and dotted lines represent the location of the primaries and equilateral triangle respectively.

3.1.3. *Out-of-plane equilibrium points*

During out-of-plane (i.e., $\alpha \neq 0, \beta = 0, \gamma \neq 0$), there exist at most eight equilibrium points (L_1, L_2, L_3, L_4, L_5, L_6, L_7, L_8) (Figure 6a). It is observed from Figure 6b that as increase the value of the $\lambda_1(= 0.05, 0.1, 0.15, 0.2, 0.3)$ and $\lambda_2 = 0.25$, the equilibrium points $L_{3,4}$ move toward primary m_1 but the equilibrium points L_2 move away from primary m_1 and the equilibrium points $L_{5,6}$ move away from $\alpha-$axis. And also as increase the value of the $\lambda_2(= 0.05, 0.1, 0.15, 0.2, 0.3)$ and $\lambda_1 = 0.25$, there exist at most eight equilibrium points (L_1, L_2, L_3, L_4, L_5, L_6, L_7, L_8) (Figure 7a). At $\lambda_2 = 0.05(Green), 0.1(Red)$, there exists six equilibrium points (Figure 7a, 7b), at $\lambda_2 = 0.15(Blue), 0.2(Magenta), 0.3(Black)$, there exists eight equilibrium points (Figure 7c). The Figure 7d is the zoomed part of the Figure 7c near the primary m_1. And observed that as increase the value of λ_2, the equilibrium points $L_{2,3,4}$ move away from origin while the equilibrium points $L_{7,8}$ move away from the primary m_1. On the other-hand, during out-of-plane (i.e., $\alpha = 0, \beta \neq 0, \gamma \neq 0$), there exist at most eleven equilibrium points $(L_1, L_2, L_3, L_4, L_5, L_6, L_7, L_8, L_9, L_{10}, L_{11})$. At$\lambda_1 = 0.05$,

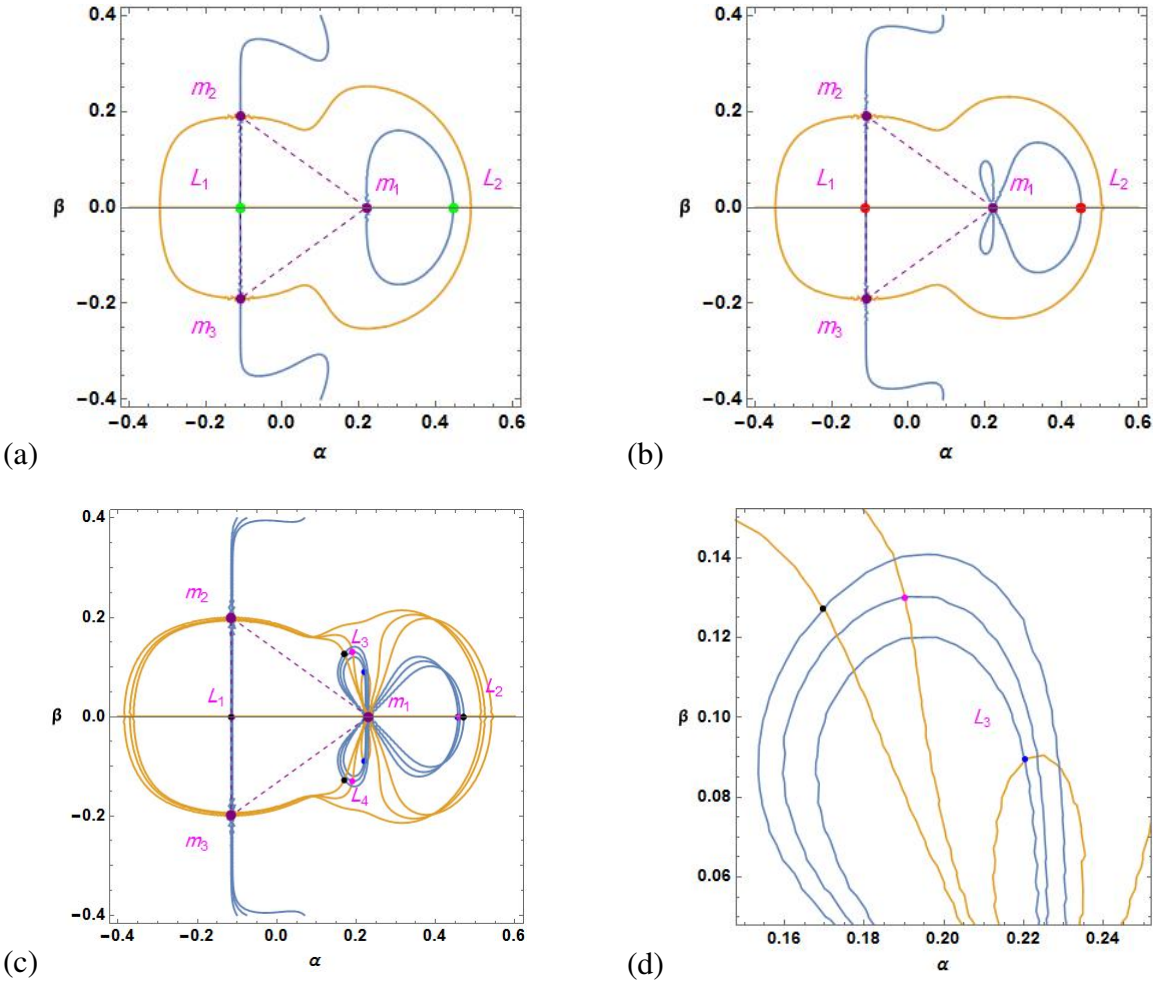

Figure 4. Locations of non-collinear equilibrium points at the values of triaxiality parameter $\lambda_1(= 0.05(Green)(a), 0.1(Red)(b), 0.15(Blue)(c), 0.2(Magenta)(c), 0.3(Black)(c))$ and $\lambda_2 = 0.25$, (d) The zoomed part of figure (c) near L_3. Purple color points represent the locations of the primaries and dotted line represent the equilateral triangular configuration.

there exist eleven equilibrium points (Figure 8a) and at $\lambda_1 = 0.1, 0.15, 0.2, 0.3$, there exist seven equilibrium points (Figure 8b). The Figure 8c is the zoomed part of Figure 8b near the origin. It is observed that the equilibrium point L_2 is at origin and $L_{1,3,4,5}$ move away from origin. And also as increase the value of the $\lambda_2(= 0.05, 0.1, 0.15, 0.2, 0.3)$ and $\lambda_1 = 0.25$, there exist at most seven equilibrium points $(L_1, L_2, L_3, L_4, L_5, L_6, L_7)$ (Figure 9a). The Figure 9b is the zoomed part of Figure 9a near the origin. And observed that as increase the value of λ_2, the equilibrium point L_2 is fixed at origin while the equilibrium points $L_{1,3,4,5}$ move away from origin.

3.2. Zero-velocity curves (ZVCs)

Equation (6) represents the Jacobi integral, where C is the Jacobi constant which is conserved. In the four-body problem when all the primaries are triaxial rigid bodies, there exist 8, 10, 12, or 14 equilibrium points depending on triaxiality parameters of the primaries.

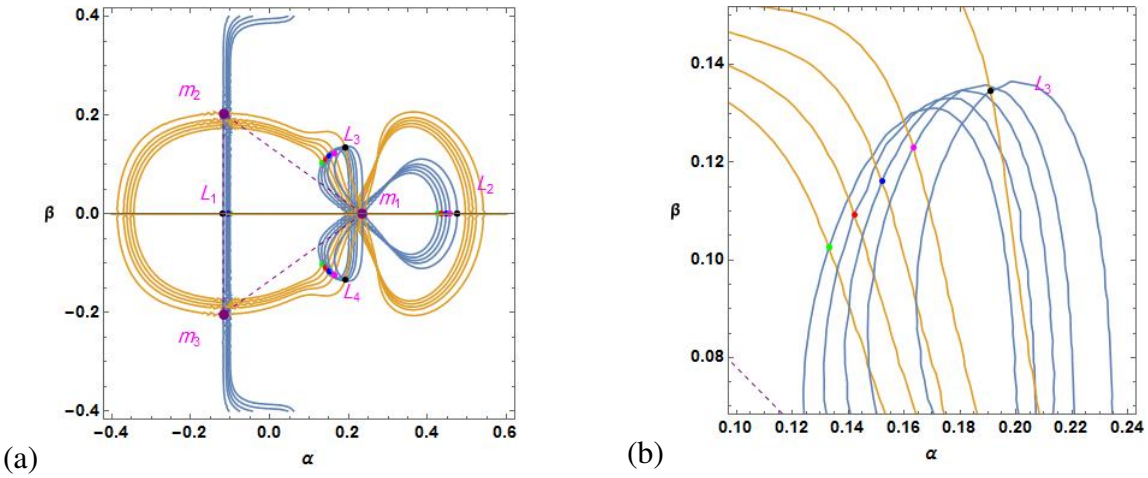

Figure 5. (a): Locations of non-collinear equilibrium points at the values of triaxiality parameter $\lambda_1 = 0.25$ and $\lambda_2 (= 0.05(Green), 0.1(Red), 0.15(Blue), 0.2(Magenta), 0.3(Black))$, (b): The zoomed part of figure (a) near L_3. Purple color points represent the locations of the primaries and dotted line represent the equilateral triangular configuration.

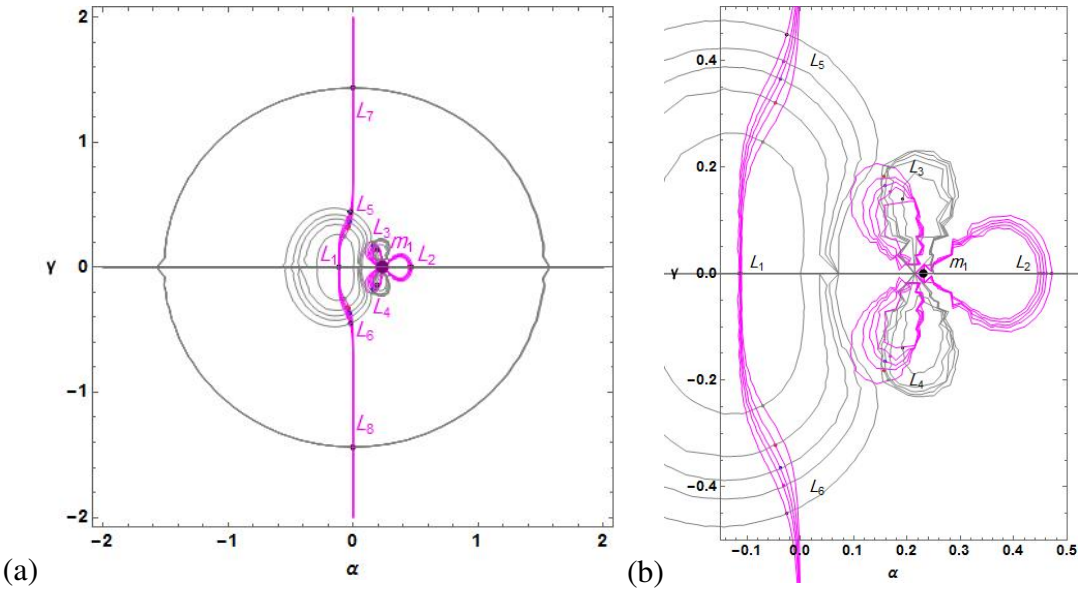

Figure 6. (a): Locations of out-of-plane equilibrium points at the values of triaxiality parameter $\lambda_1 (= 0.05(Green), 0.1(Red), 0.15(Blue), 0.2(Magenta), 0.3(Black))$ and $\lambda_2 = 0.25$, (b): The zoomed part of figure (a) near the primary m_1.

We found four equilibrium points when all the three triaxial bodies having equal mass and infinitesimal body varies its mass with time. We have plotted the zero-velocity curves for various value of Jacobian constant C at the fixed value of $\lambda_1 = 0.3, \lambda_2 = 0.25$.

From Figure 10, we observed that as the value of Jacobian constant C decreases forbidden region decreases. In the Figures 10a,b,c, pink color represent the forbidden regions and the infinitesimal body can move freely in the white regions.

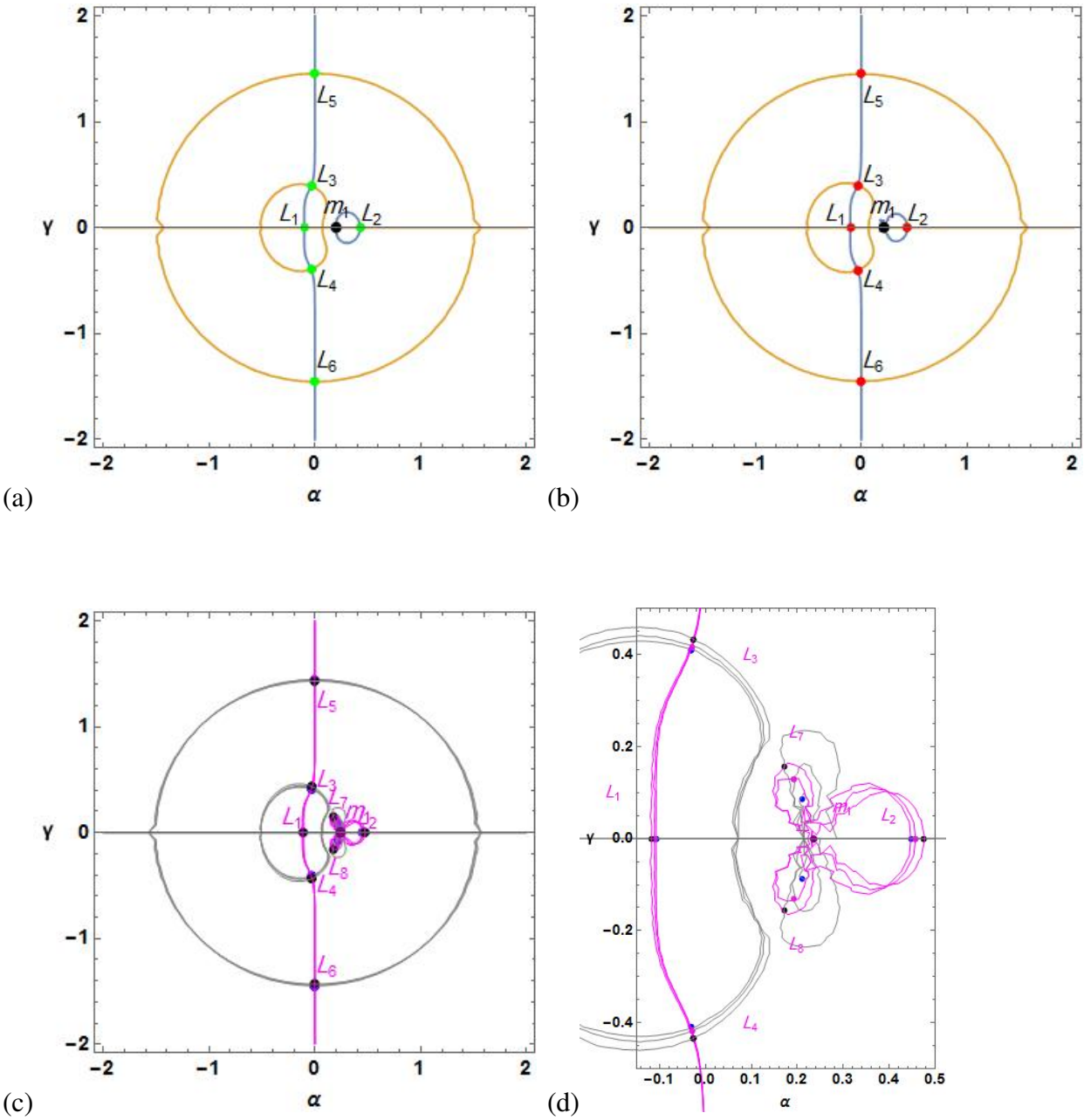

Figure 7. Locations of out-of-plane equilibrium points at the values of triaxiality parameter $\lambda_1 = 0.25$ and $\lambda_2(= 0.05(Green)(a), 0.1(Red)(b), 0.15(Blue)(c), 0.2(Magenta)(c), 0.3(Black)(c))$, (d): The zoomed part of figure (c) near m_1.

3.3. Surfaces

Here, we have drawn the zero-velocity surfaces with projections and surfaces of motion of infinitesimal body under the effect of triaxiality parameters of the primaries and the variations of mass parameter of the infinitesimal body.

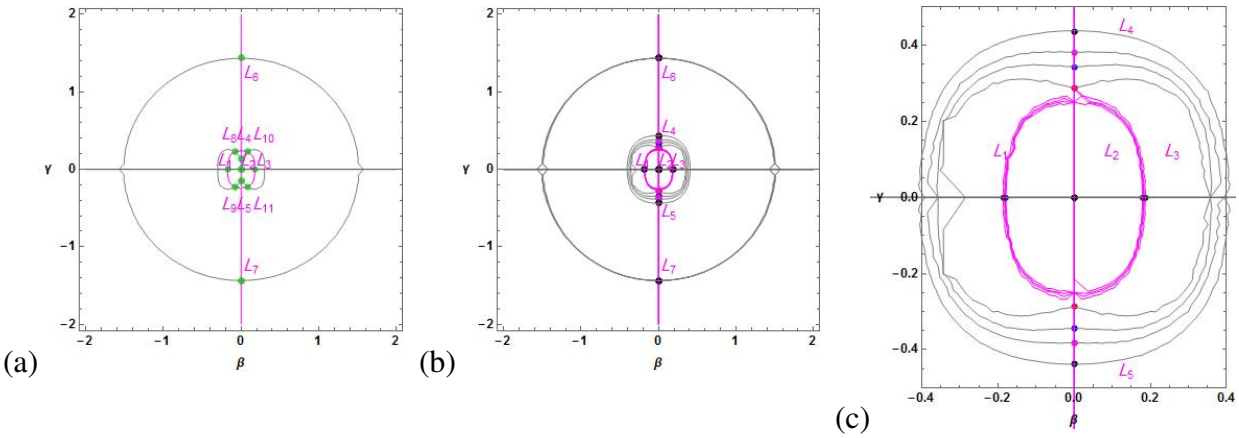

Figure 8. Locations of out-of-plane equilibrium points at the values of triaxiality parameter $\lambda_1(= 0.05(Green)(a), 0.1(Red)(b), 0.15(Blue)(b), 0.2(Magenta)(b), 0.3(Black)(b))$ and $\lambda_2 = 0.25$, (c): The zoomed part of figure (b) near origin.

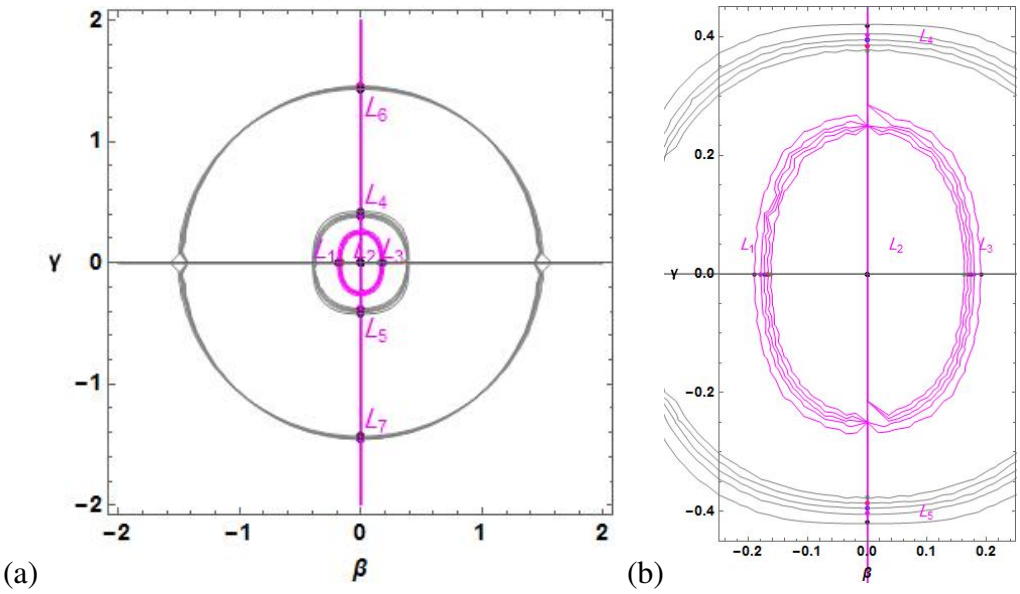

Figure 9. (a): Locations of out-of-plane equilibrium points at the values of triaxiality parameter $\lambda_1 = 0.25$ and $\lambda_2(= 0.05(Green), 0.1(Red), 0.15(Blue), 0.2(Magenta), 0.3(Black))$, (b): The zoomed part of figure (a) near origin.

3.3.1. *Zero-velocity surfaces (ZVSs)*

We have drawn the zero-velocity surfaces with projections at the fixed value of $\lambda_1 = 0.3, \lambda_2 = 0.25$. The motion is possible only inside the shaded regions and observed that the triaxiality parameters have great impact on the characteristics of the zero-velocity surfaces (Figure 11).

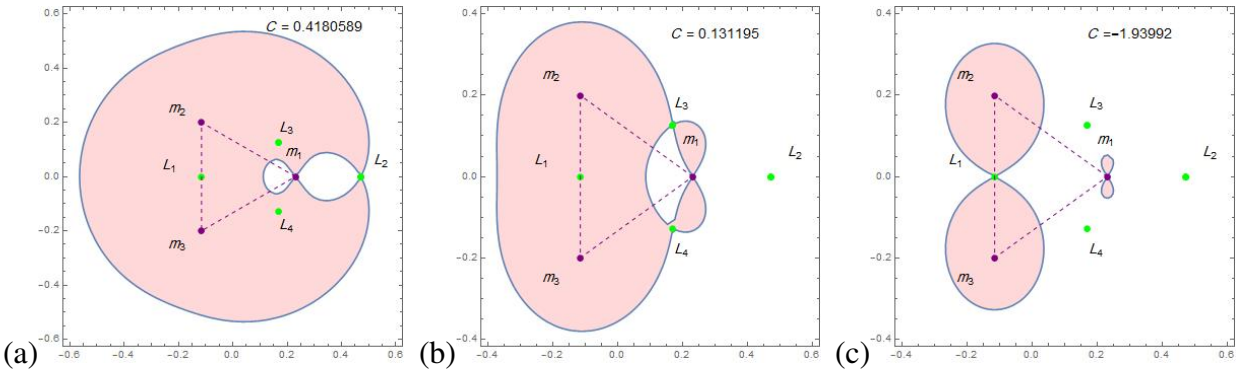

Figure 10. Zero-velocity curves at various values of Jacobi constant($C = 0.4180589(a), C = 0.1311945(b), C = -1.9399231(c)$) and at the fixed value of $\lambda_1 = 0.3, \lambda_2 = 0.25$.

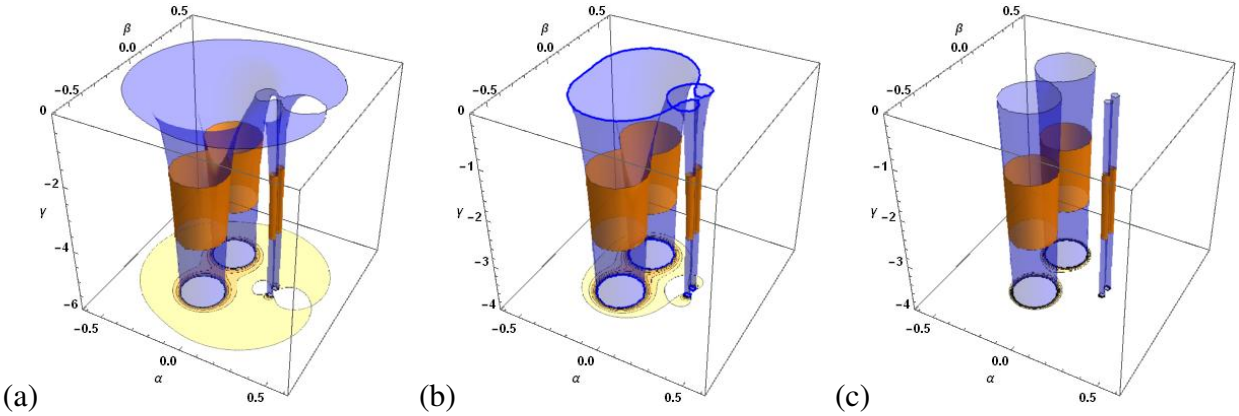

Figure 11. Zero-velocity surfaces with projections at various values of Jacobi constant($C = 0.4180589(a), C = 0.1311945(b), C = -1.9399231(c)$) and at the fixed value of $\lambda_1 = 0.3, \lambda_2 = 0.25$.

3.3.2. *Surfaces of motion of infinitesimal variable body*

We have drawn the surfaces of motion of infinitesimal variable body under the effect of triaxiality parameters ($\lambda_1 = 0.3, \lambda_2 = 0.25$.) and the variation of mass parameter ($\lambda_3 = 0.2$) of infinitesimal body. We have plotted these surfaces Figure 11a, Figure 11b and Figure 11c by considering Equations (7(a) and 7(b)), (7(a) and 7(c)) and (7(b) and 7(c)) respectively. Observe that all the surfaces appear as two connecting balloons (left balloon is big and right one is small). The motion is possible only in the shaded regions.

3.4. Newton-Raphson basins of attraction

We have studied the basins of attraction for the circular restricted four-body problem in which we have taken all the primaries as triaxial rigid body and infinitesimal body varies its mass with time. The basin of attraction or an attracting region composed by all the initial conditions that lead to a specific equilibrium points. It is an issue of great importance to get the basins of attraction which reflect some of the most important qualitative properties of the dynamical system. Using Newton-

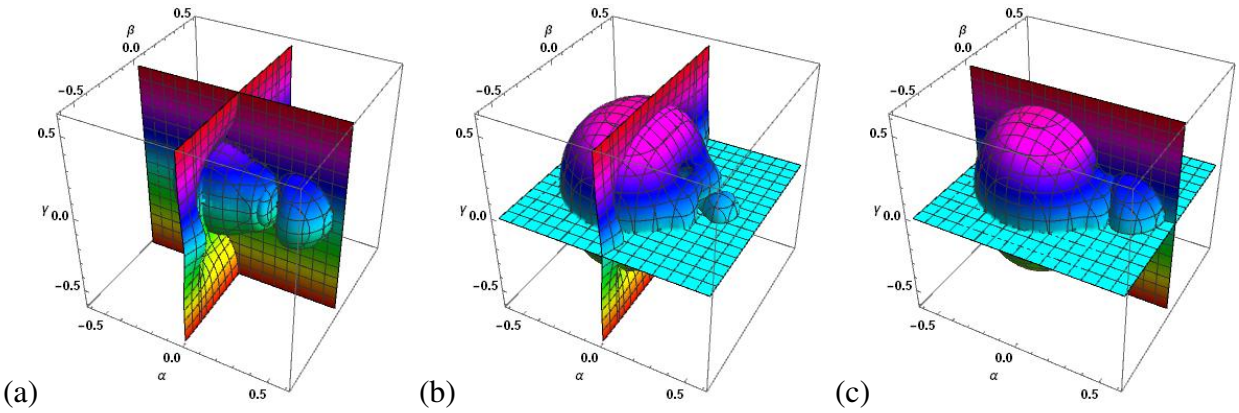

Figure 12. Surfaces of motion of infinitesimal variable body at the fixed value of $\lambda_1 = 0.3, \lambda_2 = 0.25$. (a): By considering equations 7(a) and 7(b), (b): By considering equations 7(a) and 7(c), (c): By considering equations 7(b) and 7(c).

Raphson iterative method which is very fast and simple, we have drawn the basins of attraction for five values of the triaxiality parameters ($\lambda_1 = 0.05, 0.1, 0.15, 0.2, 0.3, \lambda_2 = 0.25$). The algorithm of our problem is given by

$$\begin{cases} \alpha_{n+1} = \alpha_n - \left(\frac{\psi_\alpha \psi_{\beta\beta} - \psi_\beta \psi_{\alpha\beta}}{\psi_{\alpha\alpha}\psi_{\beta\beta} - \psi_{\alpha\beta}\psi_{\beta\alpha}}\right)_{(\alpha_n, \beta_n)}, \\ \beta_{n+1} = \beta_n - \left(\frac{\psi_\beta \psi_{\alpha\alpha} - \psi_\alpha \psi_{\beta\alpha}}{\psi_{\alpha\alpha}\psi_{\beta\beta} - \psi_{\alpha\beta}\psi_{\beta\alpha}}\right)_{(\alpha_n, \beta_n)}, \end{cases} \tag{8}$$

where α_n, β_n are the values of α and β coordinates of the n^{th} step of the Newton-Raphson iterative process.

If the initial point converges rapidly to one of the equilibrium points then this point (α, β) will be a member of the basin of attraction of the root. This process stops when the successive approximation converges to an attractor. We used color code for the classification of the equilibrium points on the $(\alpha, \beta)-$plane.

In the first and second cases when $\lambda_1 = 0.05, 0.1, \lambda_2 = 0.25$ (Figure 13 a, b),the equilibrium points L_1, L_2 represent cyan color regions. The basins of attraction corresponding to the equilibrium point L_1 extend to infinity while corresponding to the equilibrium point L_2 cover finite regions. In all the other three cases when $\lambda_1 = 0.15, 0.2, 0.3, \lambda_2 = 0.25$ (Figure 13 c, d, e), the equilibrium points L_1, L_2 represent cyan color region, L_3 represents light blue color region, and L_4 represents light green color region. The basins of attraction corresponding to the equilibrium points L_1, L_3, L_4 extend to infinity but corresponding to equilibrium point L_2 cover finite area. In this way a complete view of the basin structures created by the attractors.

We can observe in detail from the zoomed part of all the figures in Figures 13 a', b', c', d', e'. The red points and purple points in all the figures, denote the location of the equilibrium points and the primaries respectively.

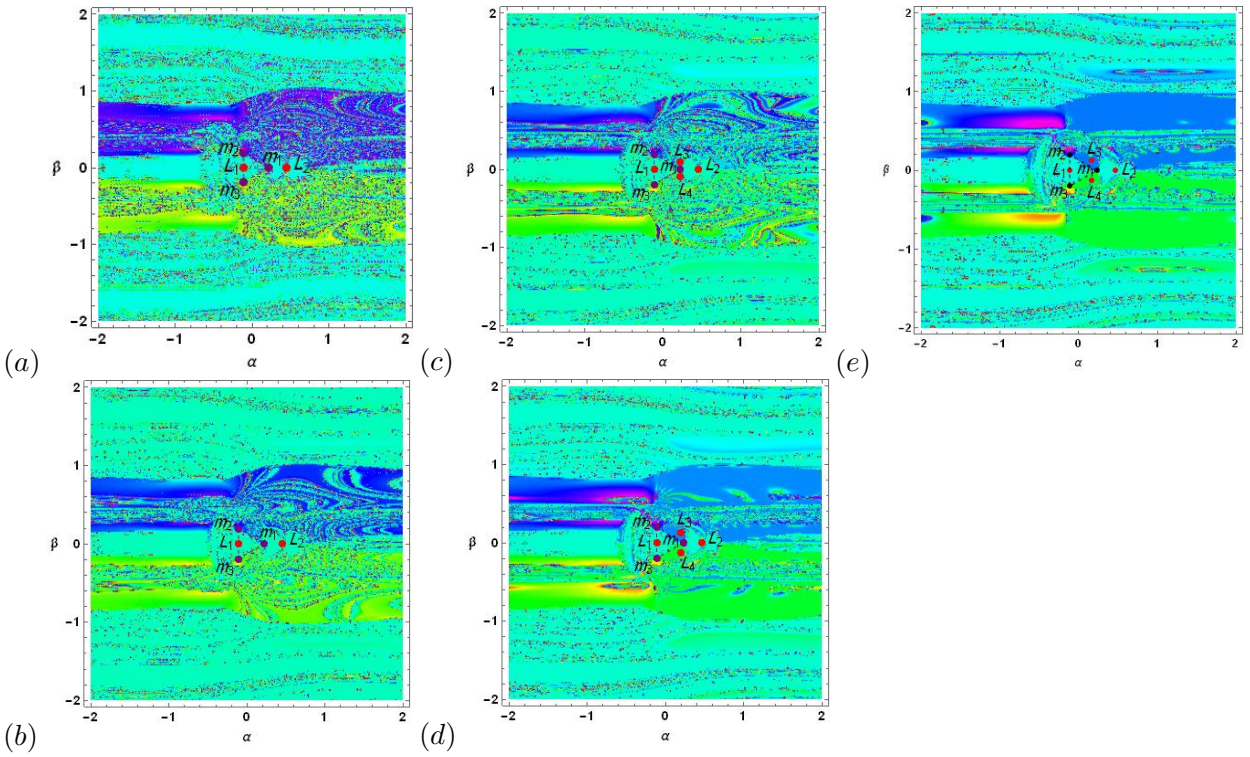

Figure 13. Newton-Raphson basins of attraction at the values of $\lambda_1 = 0.05(a), 0.1(b), 0.15(c), 0.2(d), 0.3(e), \lambda_2 = 0.25$.

4. Stability of equilibrium points

In this section, we have examined the linear stability of the equilibrium points by giving the displacements $((u, v, w) << 1)$ to $(\alpha_0, \beta_0, \gamma_0)$ as

$$\begin{cases} \alpha = u + \alpha_0, \\ \beta = v + \beta_0, \\ \gamma = w + \gamma_0, \end{cases} \tag{9}$$

where $(\alpha_0, \beta_0, \gamma_0)$ is the equilibrium point for a fixed value of time t. We can get the variational equations from the equations (5) and (9) as

$$\begin{cases} \ddot{u} - 2\dot{v} = (\psi_{\alpha\alpha})_0 u + (\psi_{\alpha\beta})_0 v + (\psi_{\alpha\gamma})_0 w, \\ \ddot{v} + 2\dot{u} = (\psi_{\beta\alpha})_0 u + (\psi_{\beta\beta})_0 v + (\psi_{\beta\gamma})_0 w, \\ \ddot{w} \quad\quad = (\psi_{\gamma\alpha})_0 u + (\psi_{\gamma\beta})_0 v + (\psi_{\gamma\gamma})_0 w, \end{cases} \tag{10}$$

where the subscript "0" in the system (10) represents the values at the equilibrium point $(\alpha_0, \beta_0, \gamma_0)$.

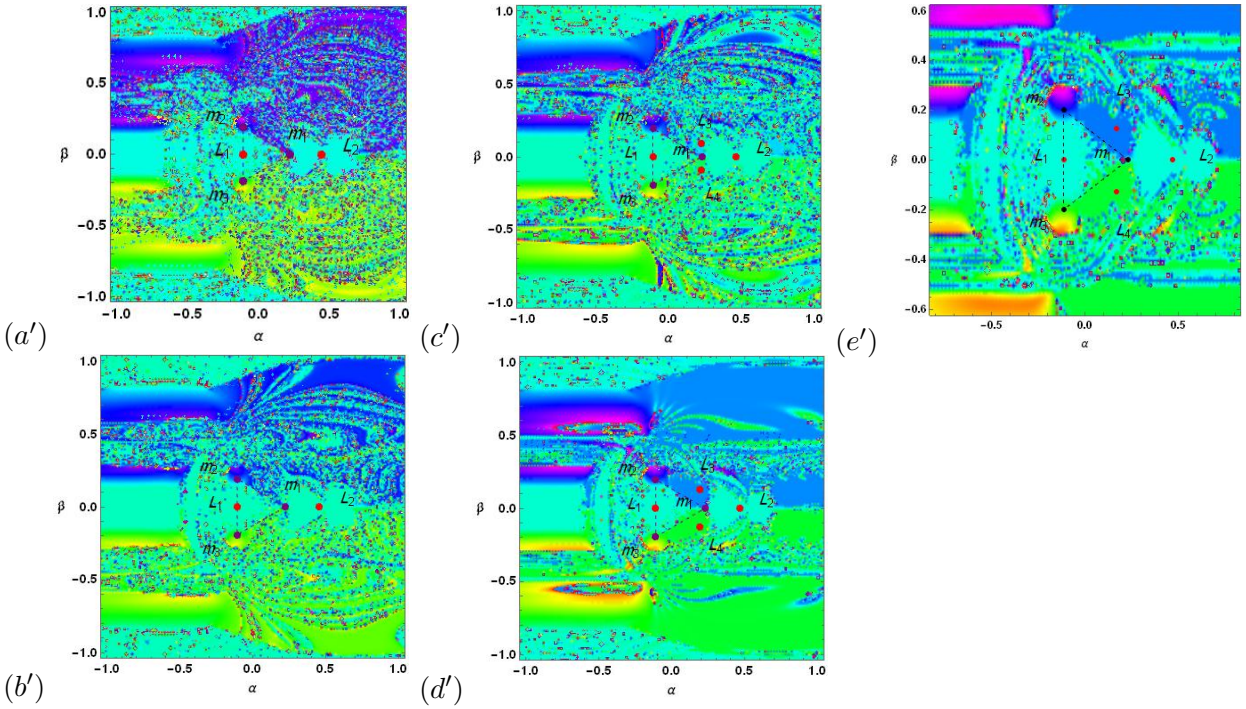

Figure 14. The zoomed part of figures $(a), (b), (c), (d), (e)$ are the figures $(a'), (b'), (c'), (d'), (e')$ near the Lagrangian configuration, respectively.

In the phase space, system (10) may be written as

$$\begin{cases} \dot{u} = u_1, \qquad \dot{v} = v_1, \qquad \dot{w} = w_1, \\ \dot{u_1} - 2v_1 = (\psi_{\alpha\alpha})_0 u + (\psi_{\alpha\beta})_0 v + (\psi_{\alpha\gamma})_0 w, \\ \dot{v_1} + 2u_1 = (\psi_{\beta\alpha})_0 u + (\psi_{\beta\beta})_0 v + (\psi_{\beta\gamma})_0 w, \\ \dot{w_1} \qquad = (\psi_{\gamma\alpha})_0 u + (\psi_{\gamma\beta})_0 v + (\psi_{\gamma\gamma})_0 w. \end{cases} \tag{11}$$

At $\lambda_3 = 0$, the system (10) reduces to a system with constant mass. For $\lambda_3 > 0$, we can not determine the linear stability from ordinary method because the distances of the primaries to the equilibrium point $(\alpha_0, \beta_0, \gamma_0)$ varies with time. Therefore, we use the Meshcherskii space-time inverse transformations.

Using the Meshcherskii inverse transformations and putting

$$x' = \epsilon^{-1/2} u,\ y' = \epsilon^{-1/2} v,\ z' = \epsilon^{-1/2} w,\ u' = \epsilon^{-1/2} u_1,\ v' = \epsilon^{-1/2} v_1,\ w' = \epsilon^{-1/2} w_1,$$

the system (11) can be written in the matrix form as follows:

$$\begin{pmatrix} \frac{dx'}{dt} \\ \frac{dy'}{dt} \\ \frac{dz'}{dt} \\ \frac{du'}{dt} \\ \frac{dv'}{dt} \\ \frac{dw'}{dt} \end{pmatrix} = A \times \begin{pmatrix} x' \\ y' \\ z' \\ u' \\ v' \\ w' \end{pmatrix}, \tag{12}$$

where

$$A = \begin{pmatrix} \frac{\lambda_3}{2} & 0 & 0 & 1 & 0 & 0 \\ 0 & \frac{\lambda_3}{2} & 0 & 0 & 1 & 0 \\ 0 & 0 & \frac{\lambda_3}{2} & 0 & 0 & 1 \\ (\psi_{\alpha\alpha})_0 & (\psi_{\alpha\beta})_0 & (\psi_{\alpha\gamma})_0 & \frac{\lambda_3}{2} & 2 & 0 \\ (\psi_{\beta\alpha})_0 & (\psi_{\beta\beta})_0 & (\psi_{\beta\gamma})_0 & -2 & \frac{\lambda_3}{2} & 0 \\ (\psi_{\gamma\alpha})_0 & (\psi_{\gamma\beta})_0 & (\psi_{\gamma\gamma})_0 & 0 & 0 & \frac{\lambda_3}{2} \end{pmatrix}.$$

As the positions of the primaries are fixed and their distances to the equilibrium points are invariable, the linear stability of (12) and (5) is consistent with each other. Thus, the linear stability of this solution depends on the existence of stable region of the equilibrium point, which in turn depends on the boundedness of the solution of linear and homogenous system of Equation (12).

The characteristic equation of the coefficient matrix A is

$$\lambda_4^6 + a_1\lambda_4^5 + a_2\lambda_4^4 + a_3\lambda_4^3 + a_4\lambda_4^2 + a_5\lambda_4 + a_6 = 0, \tag{13}$$

where $a_1 = -3\lambda_3$,

$a_2 = \frac{1}{64}(256 - 64\psi_{\alpha\alpha} - 64\psi_{\beta\beta} - 64\psi_{\gamma\gamma} + 240\lambda_3^2)$,

$a_3 = \frac{1}{64}(128\psi_{\alpha\beta} - 128\psi_{\beta\alpha} - 512\lambda_3 + 128\psi_{\alpha\alpha}\lambda_3 + 128\psi_{\beta\beta}\lambda_3 + 128\psi_{\gamma\gamma}\lambda_3 - 160\lambda_3^3)$,

$a_4 = \frac{1}{64}(-64\psi_{\alpha\beta}\psi_{\beta\alpha} + 64\psi_{\alpha\alpha}\psi_{\beta\beta} - 64\psi_{\alpha\gamma}\psi_{\gamma\alpha} - 64\psi_{\beta\gamma}\psi_{\gamma\beta} - 256\psi_{\gamma\gamma} + 64\psi_{\alpha\alpha}\psi_{\gamma\gamma}$

$+ 64\psi_{\beta\beta}\psi_{\gamma\gamma} - 192\psi_{\alpha\beta}\lambda_3 + 192\psi_{\beta\alpha}\lambda_3 + 384\lambda_3^2 - 96\psi_{\alpha\alpha}\lambda_3^2 - 96\psi_{\beta\beta}\lambda_3^2 - 96\psi_{\gamma\gamma}\lambda_3^2 + 60\lambda_3^4)$,

$a_5 = \frac{1}{64}(-128\psi_{\beta\gamma}\psi_{\gamma\alpha} + 128\psi_{\alpha\gamma}\psi_{\gamma\beta} - 128\psi_{\alpha\beta}\psi_{\gamma\gamma} + 128\psi_{\beta\alpha}\psi_{\gamma\gamma} + 64\psi_{\alpha\beta}\psi_{\beta\alpha}\lambda_3$

$- 64\psi_{\alpha\alpha}\psi_{\beta\beta}\lambda_3 + 64\psi_{\alpha\gamma}\psi_{\gamma\alpha}\lambda_3 + 64\psi_{\beta\gamma}\psi_{\gamma\beta}\lambda_3 + 256\psi_{\gamma\gamma}\lambda_3 - 64\psi_{\alpha\alpha}\psi_{\gamma\gamma}\lambda_3 - 64\psi_{\beta\beta}\psi_{\gamma\gamma}\lambda_3$

$+ 96\psi_{\alpha\beta}\lambda_3^2 - 96\psi_{\beta\alpha}\lambda_3^2 - 128\lambda_3^3 + 32\psi_{\alpha\alpha}\lambda_3^3 + 32\psi_{\beta\beta}\lambda_3^3 + 32\psi_{\gamma\gamma}\lambda_3^3 - 12\lambda_3^5)$,

$a_6 = \frac{1}{64}(64\psi_{\alpha\gamma}\psi_{\beta\beta}\psi_{\gamma\alpha} - 64\psi_{\alpha\beta}\psi_{\beta\gamma}\psi_{\gamma\alpha} - 64\psi_{\alpha\gamma}\psi_{\beta\alpha}\psi_{\gamma\beta} + 64\psi_{\alpha\alpha}\psi_{\beta\gamma}\psi_{\gamma\beta} + 64\psi_{\alpha\beta}\psi_{\beta\alpha}\psi_{\gamma\gamma}$

$- 64\psi_{\alpha\alpha}\psi_{\beta\beta}\psi_{\gamma\gamma} + 64\psi_{\beta\gamma}\psi_{\gamma\alpha}\lambda_3 - 64\psi_{\alpha\gamma}\psi_{\gamma\beta}\lambda_3 + 64\psi_{\alpha\beta}\psi_{\gamma\gamma}\lambda_3 - 64\psi_{\beta\alpha}\psi_{\gamma\gamma}\lambda_3$

$- 16\psi_{\alpha\beta}\psi_{\beta\alpha}\lambda_3^2 + 16\psi_{\alpha\alpha}\psi_{\beta\beta}\lambda_3^2 - 16\psi_{\alpha\gamma}\psi_{\gamma\alpha}\lambda_3^2 - 16\psi_{\beta\gamma}\psi_{\gamma\beta}\lambda_3^2 - 64\psi_{\gamma\gamma}\lambda_3^2 + 16\psi_{\alpha\alpha}\psi_{\gamma\gamma}\lambda_3^2$

$+ 16\psi_{\beta\beta}\psi_{\gamma\gamma}\lambda_3^2 - 16\psi_{\alpha\beta}\lambda_3^3 + 16\psi_{\beta\alpha}\lambda_3^3 + 16\lambda_3^4 - 4\psi_{\alpha\alpha}\lambda_3^4 - 4\psi_{\beta\beta}\lambda_3^4 - 4\psi_{\gamma\gamma}\lambda_3^4 + \lambda_3^6)$.

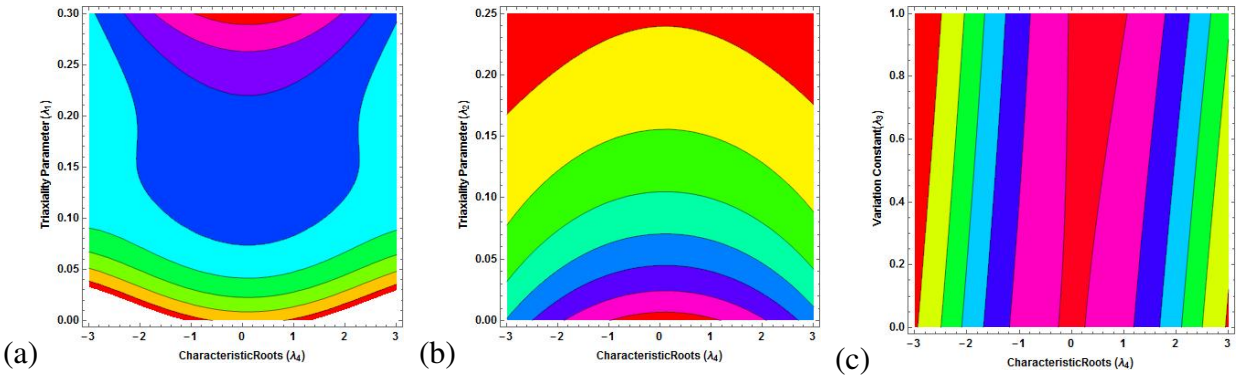

Figure 15. Stability regions (a): Characteristic root (λ_4) verses triaxiality parameter (λ_1), (b): Characteristic root (λ_4) verses triaxiality parameter (λ_2), (c): Characteristic root (λ_4) verses variation constant (λ_3).

Table 3. Coordinates of Collinear and Non-collinear equilibrium points when the primaries are triaxial rigid body with equal mass ($\lambda_2 = 0.25$).

λ_1	Equilibrium Points	Corresponding characteristic roots
0.05	(-0.110557, 0)	(-5.05844, -4.16194, 0.1 - 11.6047 I, 0.1 + 11.6047 I, **4.36194**, **5.25844**)
	(0.444717, 0)	(-1.69845, 0.1 - 1.78896 I, 0.1 + 1.78896 I, 0.1 - 1.4272 I, 0.1 + 1.4272 I, **1.89845**)
0.10	(-0.111210, 0)	(-7.33148, -6.76107, 0.1 - 16.4698 I, 0.1 + 16.4698 I, **6.96107**, **7.53148**)
	(0.450360, 0)	(-1.76407, 0.1 - 1.76572 I, 0.1 + 1.76572 I, 0.1 - 1.54554 I, 0.1 + 1.54554 I, **1.96407**)
0.15	(-0.112202, 0)	(-8.89609, -8.44743, 0.1 - 19.8473 I, 0.1 + 19.8473 I, **8.64743**, **9.09609**)
	(0.455742, 0)	(-1.81689, 0.1 - 1.63792 I, 0.1 + 1.63792 I, 0.1 - 1.74612 I, 0.1 + 1.74612 I, **2.01689**)
	(0.220206, 0.089374)	(-8.76827, 0.1 - 7.51628 I, 0.1 + 7.51628 I, 0.1 - 5.12496 I, 0.1 + 5.12496 I, **8.96827**)
	(0.220206, -0.089374)	(-8.76827, 0.1 - 7.51628 I, 0.1 + 7.51628 I, 0.1 - 5.12496 I, 0.1 + 5.12496 I, **8.96827**)
0.20	(-0.113270, 0)	(-10.097, -9.71718, 0.1 - 22.4477 I, 0.1 + 22.4477 I, **9.91718**, **10.297**)
	(0.460906, 0)	(-1.86109, 0.1 - 1.71321 I, 0.1 + 1.71321 I, 0.1 - 1.72937 I, 0.1 + 1.72937 I, **2.06109**)
	(0.190086, 0.130063)	(-3.83751, 0.1 - 2.11375 I, 0.1 + 2.11375 I, 0.1 - 4.28157 I, 0.1 + 4.28157 I, **4.03751**)
	(0.190086, -0.130063)	(-3.83751, 0.1 - 2.11375 I, 0.1 + 2.11375 I, 0.1 - 4.28157 I, 0.1 + 4.28157 I, **4.03751**)
0.30	(-0.115477, 0)	(-11.8601, -11.5596, 0.1 - 26.273 I, 0.1 + 26.273 I, **11.7596**, **12.0601**)
	(0.470703, 0)	(-1.93243, 0.1 - 1.83066 I, 0.1 + 1.83066 I, 0.1 - 1.70232 I, 0.1 + 1.70232 I, **2.13243**)
	(0.169659, 0.127267)	(-5.01066, -1.72628, 0.1 - 6.58664 I, 0.1 + 6.58664 I, **1.92628**, **5.21066**)
	(0.169659, -0.127267)	(-5.01066, -1.72628, 0.1 - 6.58664 I, 0.1 + 6.58664 I, **1.92628**, **5.21066**)

The characteristic roots of the Equation (13) have been calculated at various values of the triaxiality parameters and given in the Tables 3 and 4. We observed from the tables that we have at least one positive real root (dark black in the tables) corresponding to each equilibrium points. And also from the Figures 15 (a, b, c), we found that there are no bounded regions. Therefore, all the equilibrium points are unstable.

5. Conclusion

In the present paper, we have studied the circular restricted four-body problem with triaxial primaries having equal masses and the infinitesimal variable mass. Primaries are placed at the vertices of an equilateral triangle in the Lagrangian configuration and are moving around their common cen-

Table 4. Coordinates of Collinear and Non-collinear equilibrium points when the primaries are triaxial rigid body with equal mass ($\lambda_1 = 0.25$).

λ_2	Equilibrium Points	Corresponding Characteristic roots
0.05	(-0.100716, 0)	(-15.3998, -15.2552, 0.1 - 34.0191 I, 0.1 + 34.0191 I, **15.4552**, **15.5998**)
	(0.425624, 0)	(-1.78429, 0.1 - 1.44686 I, 0.1 + 1.44686 I, 0.1 - 1.90558 I, 0.1 + 1.90558 I, **1.98429**)
	(0.133097, 0.102523)	(-6.90196, -5.16973, 0.1 - 10.3371 I, 0.1 + 10.3371 I, **5.36973**, **7.10196**)
	(0.133097, -0.102523)	(-6.90196, -5.16973, 0.1 - 10.3371 I, 0.1 + 10.3371 I, **5.36973**, **7.10196**)
0.10	(-0.104147, 0)	(-14.1231, -13.9193, 0.1 - 31.2295 I, 0.1 + 31.2295 I, **14.1193**, **14.3231**)
	(0.436244, 0)	(-1.81407, 0.1 - 1.86281 I, 0.1 + 1.86281 I, 0.1 - 1.53107 I, 0.1 + 1.53107 I, **2.01407**)
	(0.142178, 0.109269)	(-6.19576, -4.0474, 0.1 - 8.95977 I, 0.1 + 8.95977 I, **4.2474**, **6.39576**)
	(0.142178, - 0.109269)	(-4.0474, -2.67721, -0.441126, 1.75917 - 6.88451 I, 1.75917 + 6.88451 I, **4.2474**)
0.15	(-0.107567, 0)	(-12.987, -12.7328, 0.1 - 28.747 I, 0.1 + 28.747 I, **12.9328**, **13.187**)
	(0.446443, 0)	(-1.84308, 0.1 - 1.60132 I, 0.1 + 1.60132 I, 0.1 - 1.8282 I, 0.1 + 1.8282 I, **2.04308**)
	(0.152138, 0.116128)	(-5.54914, -2.9811, 0.1 - 7.72224 I, 0.1 + 7.72224 I, **3.1811**, **5.74914**)
	(0.152138, -0.116128)	(-5.54914, -2.9811, 0.1 - 7.72224 I, 0.1 + 7.72224 I, **3.1811**, **5.74914**)
0.20	(-0.113270, 0)	(-11.9594, -11.672, 0.1 - 26.5176 I, 0.1 + 26.5176 I, **11.872**, **12.1594**)
	(0.456303, 0)	(-1.8714, 0.1 - 1.66174 I, 0.1 + 1.66174 I, 0.1 - 1.79985 I, 0.1 + 1.79985 I, **2.0714**)
	(0.163245, 0.122934)	(-4.96438, -1.87094, 0.1 - 6.60592 I, 0.1 + 6.60592 I, **2.07094**, **5.16438**)
	(0.163245, -0.122934)	(-4.96438, -1.87094, 0.1 - 6.60592 I, 0.1 + 6.60592 I, **2.07094**, **5.16438**)
0.30	(-0.117740, 0)	(-10.2454, -9.87998, 0.1 - 22.756 I, 0.1 + 22.756 I, **10.08**, **10.4454**)
	(0.475232, 0)	(-1.92623, 0.1 - 1.76256 I, 0.1 + 1.76256 I, 0.1 - 1.75697 I, 0.1 + 1.75697 I, **2.12623**)
	(0.190899, 0.134455)	(-4.04458, 0.1 - 1.87445 I, 0.1 + 1.87445 I, 0.1 - 4.6799 I, 0.1 + 4.6799 I, **4.24458**)
	(0.190899, -0.134455)	(-4.04458, 0.1 - 1.87445 I, 0.1 + 1.87445 I, 0.1 - 4.6799 I, 0.1 + 4.6799 I, **4.24458**)

ter of mass which is taken as origin. We have derived the equations of motion which are different from the classical case by the triaxiality parameters (λ_1, λ_2) and the variation of mass parameter (λ_3). Using these equations of motion, we have determined the Jacobi-integral. We have plotted equilibrium points in different planes (in-plane and out-of-plane) for the variation of the triaxial parameters and found at most eleven equilibrium points. In the next section, we have illustrated the zero-velocity curves for the different Jacobi-integral constant corresponding to the equilibrium points and observed that as decreases the value of Jacobian constant the forbidden region decreases and also in the surfaces section, we have plotted the zero-velocity surfaces for different Jacobian constant corresponding to the equilibrium points and observed that the motion of possible region is only inside the shaded region. In the surfaces of motion of infinitesimal body, we got the shapes as two connecting balloons (left one is big and right one is small) where the motion is possible.

The Newton-Raphson basins of attraction have been studied in all five cases ($\lambda_1 = 0.05, 0.1, 0.15, 0.2, 0.3$, $\lambda_2 = 0.25$) and got that as increases the value of λ_1, the configuration is expanding. These points will be clearly visible in the zoomed part of all the Figures near the lagrangian configuration. Finally, we have examined the stability of the equilibrium points in the circular restricted four-body problem for the values of the triaxiality parameters and variation of mass parameter using Meshcherskii space time inverse transformation and observed that all the equilibrium points are unstable.

We also observed that the triaxiality parameters have great impact on the motion of the infinitesimal

variable body. The corresponding results of this study are applicable in Sun-Jupiter-Asteroids-Spacecraft system.

Acknowledgement:

We are thankful to the Department of Mathematics, College of Science-Zulfi and the Deanship of Scientific research, Majmaah University, Kingdom of Saudi Arabia for providing all the research facilities to complete this research work.

REFERENCES

Abdullah (2014). Periodic orbits around Lagrangian points of the circular restricted four-body problem, Invertis Journal of Science and Technology, Vol. 7, No. 1, pp. 29–38.

Abouelmagd, E. I. and Mostafa, A. (2015). Out of plane equilibrium points locations and the forbidden movement regions in the restricted three-body problem with variable mass, Astrophys. Space Sci., Vol. 357, No. 58. doi:10.1007/s10509-015-2294-7.

Ansari, A. A. (2016(a)). Stability of the equilibrium points in the photogravitational circular restricted four-body problem with the effect of perturbations and variable mass, Science International (Lahore), Vol. 28, pp. 859–866.

Ansari, A. A. (2016(b)). Stability of the equilibrium points in the circular restricted four-body problem with oblate primary and variable mass, International Journal of Advanced Astronomy, Vol. 4, No. 1, pp. 14–19.

Ansari, A. A. (2016(c)). The Photogravitational Circular Restricted Four-body Problem with Variable Masses, Journal of Engineering and Applied Sciences, Vol. 3, No. 2, pp. 30–38.

Ansari, A. A. (2017(a)). The circular restricted four-body problem with variable masses, Nonlinear Sci. Lett. A, Vol. 8, No. 3, pp. 303–312.

Ansari, A. A. (2017(b)). Effect of Albedo on the motion of the infinitesimal body in circular restricted three-body problem with variable masses, Italian J. of Pure and Applied Mathematics, Vol. 38, pp. 581–600.

Ansari, A. A., Alhussain, Z. A. and Prasad, S. (2018). Circular restricted three-body problem when both the primaries are heterogeneous spheroid of three layers and infinitesimal body varies its mass, J. of Astrophys. Astr., Vol. 39, No. 57.

Asique, M. C., Suraj, M. S. and Hasan, M. R. (2015(a)). On the R4BP when third primary is an oblate spheroid, Astrophys. Space Sci., Vol. 357, No. 82. doi:10.1007/s10509-015-2235-5.

Asique, M. C., Suraj, M. S. and Hasan, M. R. (2015(b)). On the photogravitational R4BP when the third primary is an oblate/prolate spheroid, Astrophys. Space Sci., Vol. 360, No. 13. doi:10.1007/s10509-015-2522-1.

Asique, M. C., Suraj, M. S. and Hasan, M. R. (2016). On the photogravitational R4BP when the third primary is a triaxial rigid body, Astrophys. Space Sci., Vol. 361, No. 379. doi:10.1007/s10509-016-2959-x.

Asique, M. C., Suraj, M. S. and Hasan, M. R. (2017). On the R4BP when Third Primary is an Ellipsoid. Journal of Astronaut. Sci., Vol. 64, pp. 231–250. doi:10.1007/s40295-016-0104-2.

Baltagiannis, A. and Papadakis, K. E. (2011). Equilibrium points and their stability in the restricted four body problem, International Journal of Bifurcation and Chaos, Vol. 21, No. 8, pp. 2179–2193. doi:10.1142/S0218127411029707.

Douskos, C. N. (2010). Collinear equilibrium points of Hill's problem with radiation pressure and oblateness and their fractal basins of attraction, Astrophys. Space Sci., Vol. 326, pp. 263–271.

Hadjidemetriou, J. D. (1980). The Restricted Planetary 4-Body Problem, Celest. Mech., Vol. 21, pp. 63–71.

Jeans, J. H. (1928). *Astronomy and Cosmogony*, Cambridge University Press, Cambridge.

Kalvouridis, T. J. (1997). The oblate spheroids version of the restricted photogravitational $2+2$ body problem, Astrophys. Space Sci., Vol. 246, No. 2, pp. 219–227.

Kalvouridis, T. J., Arribas, M. and Elipe, A. (2006). Dynamical properties of the restricted four-body problem with radiation pressure, Mechanics research communications, Vol. 33, pp. 811–817.

Kalvouridis, T. J. and Mavraganis, A. G. (1995). Equilibria and stability of the restricted photogravitational problem of $2+2$ bodies, Astrophys. Space Sci., Vol. 226, No. 1, pp. 137–148.

Kumari, R. and Kushvah, B. S. (2013). Equilibrium Points and Zero Velocity Surfaces in the Restricted Four Body Problem with Solar Wind Drag, Astrophys. Space Sci., Vol. 344, pp. 347–359.

Kumari, R. and Kushvah, B. S. (2014). Stability regions of equilibrium points in the restricted four body problem with oblateness effects, Astrophys. Space Sci., Vol. 349, pp. 693–704.

Lichtenegger, H.(1984). The dynamics of bodies with variable masses, Celest. Mech., Vol. 34, pp. 357–368.

Lukyanov, L. G. (2009). On the restricted circular conservative three-body problem with variable masses, Astronomy Letters, Vol. 35, No. 5, pp. 349–359.

Meshcherskii, I. V. (1952). *Works on the Mechanics of Bodies of Variable Mass*, GITTL, Moscow.

Mittal, A., Aggrawal, R., Suraj, M. S. and Bist, A. (2016). Stability of libration points in the restricted four-body problem with variable mass, Astrophys. Space sci., Vol. 361, No. 329. doi:10.1007/s10509-016-2901-2

Pandey, L. P. and Ahmad, I. (2013). Periodic orbits and bifurcations in the Sitnikov four-body problem when all primaries are oblate, Astrophys. Space sci., Vol. 345, pp. 73–83. doi:10.1007/s10509-013-1375-8

Papadakis, K. E. (2016). Families of three-dimensional periodic solutions in the circular restricted four-body Problem, Astrophys. Space Sci., Vol. 361, No. 129.

Papadouris, J. P. and Papadakis, K. E. (2013). Equilibrium points in the photogravitational restricted four-body Problem, Astrophys. Space Sci., Vol. 344, pp. 21–38.

Papadouris, J. P. and Papadakis, K. E. (2014). Periodic solutions in the photogravitational restricted four-body problem, MNRAS, Vol. 442, pp. 1628–1639.

Shrivastava, A. K. and Ishwar, B. (1983). Equations of motion of the restricted problem of three bodies with variable mass, Celest. Mech., Vol. 30, pp. 323–328.

Simo, C. (1978). Relative equilibrium solutions in the four body problem, Celest. Mech., Vol. 18, pp. 165–184.

Singh, J. and Ishwar, B. (1984). Effect of perturbations on the location of equilibrium points in the restricted problem of three bodies with variable mass, Celest. Mech., Vol. 32, pp. 297–305.

Singh, J. and Ishwar, B. (1985). Effect of perturbations on the stability of triangular points in the restricted problem of three bodies with variable mass, Celest. Mech., Vol. 35, pp. 201–207.

Singh, J. (2003). Photogravitational restricted three body problems with variable mass, Indian Journal of Pure and Applied Math, Vol. 32, No. 2, pp. 335–341.

Singh, J. and Leke, O. (2010). Stability of photogravitational restricted three body problem with variable mass, Astrophys. Space Sci., Vol. 326, No. 2, pp. 305–314.

Singh, J. and Leke, O. (2013). Existence and Stability of Equilibrium Points in the Robe's Restricted Three-Body Problem with Variable Masses, International Journal of Astronomy and Astrophysics, Vol. 3, pp. 113–122. http://dx.doi.org/10.4236/ijaa.2013.32013.

Singh, J. and Vincent, A. E. (2016(a)). Equilibrium points in the restricted four-body problem with radiation pressure, Few-Body Syst., Vol. 57, pp. 83–91.

Singh, J. and Vincent, A. E. (2016(b)). Out-of-plane equilibrium points in the photogravitational restricted four-Body problem with oblateness, British Journal of Mathematics and Computer Science, Vol. 19, No. 5, pp. 1–15.

Suraj, M. S., Hasan, M. R. and Asique, M. C. (2017). Fractal basins of attraction in the restricted four-body problem when the primaries are triaxial rigid bodies, Astrophys. Space Sci., Vol. 362, No. 211.

Zhang, M. J., Zhao, C. Y. and Xiong, Y. Q. (2012). On the triangular libration points in photogravitational restricted three body problem with variable mass, Astrophys. Space Sci., Vol. 337, pp. 107–113. doi:10.1007/s10509- 011-0821-8.

Zotos, E. E. (2016(a)). Fractal basins of attraction in the planar circular restricted three body problem with oblateness and radiation pressure, Astrophys. Space Sci., Vol. 181, No. 17.

Zotos, E. E. (2016(b)). Fractal basins boundaries and escape dynamics in a multi-well potential, Non-linear Dyn., Vol. 85, pp. 1613–1633.

Zotos, E. E. (2016(c)). Investigating the Newton-Raphson basins of attraction in the restricted three body problem with modified Newtonian gravity, J. Appl. Math. Comput., pp. 1–19.

Zotos, E. E. (2017). Revealing the basins of convergence in the planar equilateral restricted four-body problem, Astrophys. Space Sci., Vol. 362, No. 2.

Zotos, E. E. and Suraj, M. S. (2018). Basins of attraction of equilibrium points in the planar circular restricted five-body problem, Astrophys. Space Sci., Vol. 363, No. 20.